ft Value of O^{14} and the Universality of the Fermi Interaction*

R. K. BARDIN, C. A. BARNES, W. A. FOWLER, AND P. A. SEEGER
California Institute of Technology, Pasadena, California

(Received March 13, 1962)

The conserved-vector-current theory of the strangeness-conserving weak decays predicts that G_V, the vector coupling constant in nuclear beta decay, should be equal to G_μ, the coupling constant in the muon decay. To make possible a more precise comparison of G_V and G_μ, the ft value of O^{14} has been remeasured. The end-point energy of the positron decay has been determined by measuring the Q values of the reactions $C^{12}(He^3,n)O^{14}$ and $C^{12}(He^3,p)N^{14*}$ (2.311-MeV state), using the same techniques and equipment where possible in order to minimize the uncertainty in the difference of the Q values. The results of these measurements are $Q_n=-1148.8\pm0.6$ keV and $Q_p=2468.4\pm1.0$ keV, which yield $E_{max}(\beta^+)=1812.6\pm1.4$ keV, all energies relative to the $Li^7(p,n)Be^7$ threshold assumed as 1880.7 ± 0.4 keV. The half-life of O^{14} has also been remeasured as 71.00 ± 0.13 sec, which implies a partial half-life of 71.43 ± 0.15 sec for the transition to the 2.311-MeV state of N^{14}. Averaged with the recent half-life measurement of Hendrie and Gerhart, we obtain an ft value of 3075 ± 10 sec for the O^{14} decay, after correcting for nuclear form factors, electron screening, and K-capture competition. With the radiative corrections of Kinoshita and Sirlin, the value obtained for G_V is $(1.4025\pm0.0022)\times10^{-49}$ erg-cm^3, where the quoted error is experimental in origin. This is to be compared with the value computed from recent muon decay measurements, $G_\mu=(1.4312\pm0.0011)\times10^{-49}$ erg-cm^3, which is $(2.0\pm0.2)\%$ larger. As there appear to be several possible theoretical explanations for this small discrepancy, the present results are consistent with the conserved-vector-current hypothesis.

1. INTRODUCTION

THE experimentally observed near equality of the coupling constants in the nuclear beta decay and in muon decay has suggested the attractive idea that all of the so-called "weak interactions" proceed by a universal Fermi interaction.[1] However, as the virtual states of the nucleon wherein it has emitted a charged pion would not be expected to undergo beta decay in the simple fashion of the usual theory, the fact that the existence of these virtual states does not produce a considerable reduction in the coupling constant for nuclear beta decay requires an explanation. This explanation is elegantly furnished by the conserved-vector-current hypothesis of Feynman and Gell-Mann.[1,2]

The proposal of this interesting hypothesis has stimulated further study of the electromagnetic and other small corrections to these decay processes,[3–6] and raised considerable interest in establishing the exact degree of equality of the coupling constants G_V, for the vector nuclear beta decay, and G_μ, for the muon decay, when these corrections are taken into consideration. Recent measurements of the muon mean life[7,8] and muon mass[9–11] have considerably improved the precision of our knowledge of G_μ, making desirable a similar improvement in the value of G_V. Of the various experiments yielding a determination of this quantity, a measurement of the ft value of the $0^+\rightarrow0^+$ beta transition $O^{14}(\beta^+,\nu)N^{14*}$ (2.311-MeV state) seemed the most satisfactory from the point of view of the state of the theoretical calculations.[6]

Due to the high-order dependence of f on the end-point energy of the positron spectrum, and the experimental difficulty of obtaining a sufficiently accurate determination of this end-point energy from beta spectrum measurements,[12,13] the mass difference of O^{14} and N^{14*}, the parent and daughter states of the beta decay, is best obtained in a somewhat more indirect manner. Previous workers have determined this mass difference by measuring the neutron threshold for the reaction $C^{12}(He^3,n)O^{14}$, which gives the mass difference $O^{14}-C^{12}$ in terms of the relatively well-known masses of the neutron and He^3 atom (see, however, the discussion of the He^3 mass below), and combining this result with a determination of the mass difference $N^{14*}-C^{12}$ from various tabulated reaction cycles and mass doublets.

Bromley *et al.*[14] have measured the neutron threshold as $E_{th}=1449.6\pm2.8$ keV relative to the $Li^7(p,n)Be^7$ threshold assumed as 1881.6 ± 0.45 keV, which yields a Q value for the $C^{12}(He^3,n)O^{14}$ reaction of -1158.5 ± 3 keV. Using the adjusted Q values and mass defects tabulated by Mattauch *et al.*[15] for the $N^{14}-C^{12}$ mass difference, and the value of Bockelman *et al.*[16] for the N^{14*} excitation (2313 ± 5 keV), they calculated $E_{max}(\beta^+)=1809.7\pm7.8$ keV.

* Supported in part by the Joint Program of the Office of Naval Research and the U. S. Atomic Energy Commission.

[1] R. P. Feynman and M. Gell-Mann, Phys. Rev. **109**, 193 (1958).
[2] M. Gell-Mann, Phys. Rev. **111**, 362 (1958).
[3] R. E. Behrends, R. J. Finkelstein, and A. Sirlin, Phys. Rev. **101**, 866 (1956).
[4] S. M. Berman, Phys. Rev. **112**, 267 (1958).
[5] T. Kinoshita and A. Sirlin, Phys. Rev. **113**, 1652 (1959).
[6] L. Durand, L. F. Landowitz, and R. B. Marr, Phys. Rev. Letters **4**, 620 (1960).
[7] R. A. Reiter, T. A. Romanowski, R. B. Sutton, and B. G. Chidley, Phys. Rev. Letters **5**, 22 (1960).
[8] V. L. Telegdi, R. A. Swanson, R. A. Lundy, and D. D. Yovanovitch, quoted in references 6 and 7 above.
[9] J. Lathrop, R. A. Lundy, S. Penman, V. L. Telegdi, R. Winston, D. D. Yovanovitch, and A. J. Bearden, Nuovo cimento **17**, 114 (1960).
[10] S. Devons, G. Gidal, L. M. Lederman, and G. Shapiro, Phys. Rev. Letters **5**, 330 (1960).
[11] G. Charpak, F. J. M. Farley, R. L. Garwin, T. Muller, J. C. Sens, V. L. Telegdi, and A. Zichichi, Phys. Rev. Letters **6**, 128 (1961).
[12] J. B. Gerhart, Phys. Rev. **95**, 288 (1954).
[13] J. R. Penning and F. H. Schmidt, Phys. Rev. **94**, 779A (1954).
[14] D. A. Bromley, E. Almqvist, H. E. Gove, A. E. Litherland, E. B. Paul, and A. J. Ferguson, Phys. Rev. **105**, 957 (1957).
[15] J. Mattauch, L. Waldmann, R. Bieri, and F. Everling, Z. Naturforsch. **11a**, 525 (1956).
[16] C. K. Bockelman, C. P. Browne, W. W. Buechner, and A. Sperduto, Phys. Rev. **92**, 665 (1953).

The group at the Naval Research Laboratory have obtained threshold values $E_{th}=1435\pm5$ keV[17] and $E_{th}=1436.2\pm0.9$ keV.[18,19] The first of these measurements was taken with a 90° magnetic analyzer calibrated with the $Li^7(p,n)Be^7$ threshold at 1881.1 keV, while the second was an absolute measurement with the NRL 2-m electrostatic analyzer. Bondelid *et al.*[18] combined their Q value for the $C^{12}(He^3,n)O^{14}$ reaction with values from the tables of Mattauch *et al.*[15] and the value 2312 ± 1.2 keV for the excitation of N^{14*}, taken from Ajzenberg-Selove and Lauritsen,[20] to get $E_{max}(\beta^+)=1800.0\pm1.2$ keV. Since the publication of the preliminary report of the present experiment,[21] Butler and Bondelid[19] have reevaluated their data, using masses from the tables of Everling *et al.*,[22] which are in much better agreement with the measured Q values from the present experiment. Their recalculated value of the positron end-point energy is $E_{max}(\beta^+)=1809.7\pm1.5$ keV.

2. CHOICE OF EXPERIMENT

A comparison of the 1960 atomic mass tables[22] with the 1956 tables[15] shows disturbingly large changes in masses important for this experiment. The mass excess of He^3 changed from 15.8144 ± 0.0042 MeV[15] to 15.8190 ± 0.0002 MeV[22] (O^{16} scale), an increase of 4.6 keV. The calculated Q value for the reaction $C^{12}(He^3,p)N^{14}$ changed by 10.8 keV from 4.7678 MeV[15] to 4.7786 MeV.[22] Considering, in addition, the poor agreement of the various measurements of the $C^{12}(He^3,n)O^{14}$ threshold energy,[14,17–19] we decided to reduce as much as possible the dependence of the positron end-point energy on subsidiary measurements by measuring the mass difference of O^{14} and N^{14*} directly in the reactions,

$$C^{12}+He^3\rightarrow O^{14}+n+Q_n, \tag{1}$$

$$C^{12}+He^3\rightarrow N^{14*}+H^1+Q_p. \tag{2}$$

To evaluate $E_{max}(\beta^+)$ from these two Q values, the only masses which need to be known with high precision are the electron mass[23] and the neutron–hydrogen atom mass difference.[22]

$$\begin{aligned}E_{max}(\beta^+)&=(O^{14}-N^{14*})c^2-2m_ec^2\\&=Q_p-Q_n+(H^1-n)c^2-2m_ec^2\\&=Q_p-Q_n-1804.6\pm0.5\text{ keV}.\end{aligned} \tag{3}$$

The quoted errors are standard deviations, here and in all results from this laboratory given below. It should be noted that the value used for $(n-H^1)c^2$, 782.61 ± 0.40 keV, has recently been confirmed by the NRL group, who get 782.9 ± 0.4 keV from an absolute measurement of the $T^3(p,n)He^3$ threshold energy.[24]

To complete the ft value measurement, it seemed desirable to remeasure the half-life of O^{14}, if possible with smaller error than that of the measurement by Gerhart,[12] $t=72.1\pm0.4$ sec. It was decided to adopt the value given by Sherr *et al.*[25] for the ground-state branching ratio of the decay, $(0.60\pm0.10)\%$, since the quoted error does not make a large contribution to the error of the partial half-life to the N^{14*} excited state.

The primary energy calibration for the experiment was chosen as the $Li^7(p,n)Be^7$ threshold, assumed as 1880.7 ± 0.4 keV, in accord with the recent recommendation of Marion.[26] This value is in good agreement with the recent measurement of Beckner *et al.*,[27] 1880.5 ± 0.8 keV.

3. EXPERIMENTAL ARRANGEMENT

The experiment was carried out using the Kellogg Radiation Laboratory 3.2-MV electrostatic accelerator, 90° electrostatic analyzer, and 16-in.-radius double-focusing magnetic spectrometer, with modifications to accessory equipment to provide extra accuracy and flexibility. The electrostatic analyzer is that described by Fowler, Lauritsen, and Lauritsen,[28] with modifications of power supply and control circuits to extend its range for operation with the 3.2-MV accelerator; the magnetic spectrometer is described in the thesis of Li.[29]

3.1. $C^{12}(He^3,p)N^{14*}$ (2.311-MeV State)

The low yield of this reaction at the threshold for $C^{12}(He^3,n)O^{14}$ ruled out the attractive idea of measuring both reactions at the same energy of bombardment. It therefore seemed advisable to look for a scheme which would permit the calibration of the magnetic spectrometer at the field setting and observation angle actually to be used in the reaction energy measurement, thus eliminating the effects of the known spectrometer nonlinearity,[29] but with the restriction that the reaction yield at the selected bombarding energy and observation angle should be reasonably large, and yet have small derivatives in energy and angle. This last restriction is necessary to avoid a complicated and rather

[17] J. W. Butler, Bull. Am. Phys. Soc. **1**, 94 (1956).
[18] R. O. Bondelid, J. W. Butler, C. A. Kennedy, and A. del Callar, Naval Research Laboratory Quarterly on Nuclear Science and Technology, January 1960 (unpublished), p. 7.
[19] J. W. Butler and R. O. Bondelid, Phys. Rev. **121**, 1770 (1961).
[20] F. Ajzenberg-Selove and T. Lauritsen, Nuclear Phys. **11**, 1 (1959).
[21] R. K. Bardin, C. A. Barnes, W. A. Fowler, and P. A. Seeger, Phys. Rev. Letters **5**, 323 (1960).
[22] F. Everling, L. A. König, J. H. E. Mattauch, and A. H. Wapstra, Nuclear Phys. **18**, 529 (1960).
[23] E. R. Cohen, J. W. M. DuMond, T. W. Layton, and J. S. Rollett, Revs. Modern Phys. **27**, 363 (1955).
[24] R. O. Bondelid, J. W. Butler, C. A. Kennedy, and A. del Callar, Phys. Rev. **120**, 887 (1960).
[25] R. Sherr, J. B. Gerhart, H. Horie, and W. F. Hornyak, Phys. Rev. **100**, 945 (1955).
[26] J. B. Marion, Revs. Modern Phys. **33**, 139 (1961).
[27] E. H. Beckner, R. L. Bramblett, G. C. Phillips, and T. A. Eastwood, Phys. Rev. **123**, 2100 (1961).
[28] W. A. Fowler, C. C. Lauritsen, and T. Lauritsen, Rev. Sci. Instr. **18**, 818 (1947).
[29] C. W. Li, Ph.D. thesis, California Institute of Technology, 1951 (unpublished).

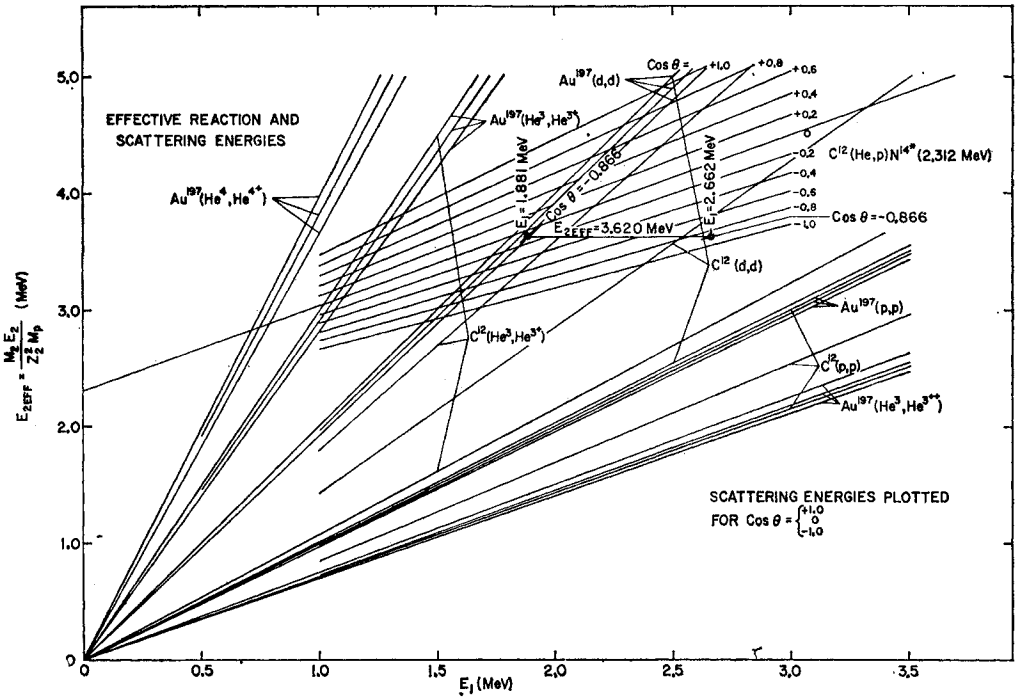

FIG. 1. Plot of spectrometer setting $E_{2\text{eff}}$, defined as $M_2E_2/Z_2^2M_p$, vs bombarding energy E_1 for the reaction $C^{12}(He^3,p)N^{14*}$ (2.311-MeV state) and for various elastic scattering processes. The elastic scattering of deuterons by gold at an incident energy of 1.88 MeV, and the reaction $C^{12}(He^3,p)N^{14*}$ at an incident energy of 2.66 MeV, both give $E_{2\text{eff}}=3.62$ MeV at $\theta_{\text{lab}}=150°$.

difficult analysis of the yield profile (the graph of the reaction proton yield vs bombarding energy).[30] As the angular resolution $\Delta\theta$ of the spectrometer contributes to the width of the rise of the profile in proportion to $(\partial E_2/\partial\theta)\Delta\theta$, where E_2 is the emerging proton energy, the precision with which one can locate the rise is also improved by doing the measurement at an angle as far from 90° in the laboratory as possible, since $\partial E_2/\partial\theta$ has maximum value at that angle.[31]

A plot was therefore constructed of the "effective energy" of the emerging particle as referred to protons in the magnetic spectrometer, $E_{2\text{eff}}=M_2E_2/Z_2^2M_p$, vs bombarding energy E_1 and observation angle θ for various elastic scattering processes, on the same axes as a similar plot for the $C^{12}(He^3,p)N^{14*}$ reaction (Fig. 1). It was hoped that the known kinematics of one of the scattering processes could be used to transfer the 1880.7-keV calibration point of the electrostatic analyzer to the magnetic spectrometer at an energy and angle satisfying the above requirements. This proved to be possible by making use of the flexibility of the four-way ion-source gas system in the terminal of the accelerator, which permits rapid selection of H_2, D_2, He^3, or He^4 as the ion-source gas.

The chosen sequence of operations was as follows. After the primary calibration of the electrostatic analyzer at the $Li^7(p,n)Be^7$ threshold, the magnetic spectrometer was calibrated precisely at a setting corresponding to a proton energy of about 3.63 MeV, and at a laboratory angle of 150°, with $Au^{197}(d,d)Au^{197}$ elastic scattering. As this process involved changing the electrostatic analyzer setting only over a small range near the primary calibration energy, the resulting magnetic spectrometer calibration was essentially independent of possible nonlinearity of the electrostatic analyzer. The generator voltage was then raised to about 2.69 MV to produce protons from the $C^{12}(He^3,p)N^{14*}$ reaction at the 3.63-MeV calibration energy of the magnetic spectrometer. The scheme is illustrated in Fig. 1.

Care was taken in the performance of the experiment to give the equipment every opportunity to reach thermal equilibrium; the magnetic spectrometer, in particular, was carefully maintained at constant field throughout the experiment to minimize the effects of both thermal and magnetic hysteresis. The electrostatic analyzer was used to make all extrapolations away from the calibration points. To minimize the effects of long-term drifts on the result, the calibrations were repeated in reversed order after each run of the $C^{12}(He^3,p)N^{14*}$ reaction.

The detector used for the protons at the focus of the magnetic spectrometer was a 0.003-in. thick CsI scintillator mounted on a DuMont 6291 photomultiplier

[30] R. K. Bardin, Ph.D. thesis, California Institute of Technology, 1961 (unpublished).
[31] A. B. Brown, C. W. Snyder, W. A. Fowler, and C. C. Lauritsen, Phys. Rev. 82, 159 (1951).

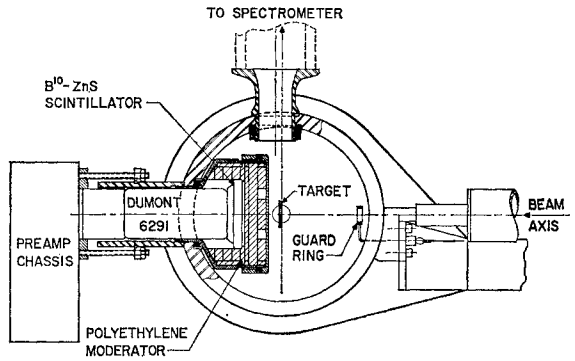

FIG. 2. The neutron scintillation counter mounted in the variable-angle target chamber. This geometrical arrangement of target, moderator, and scintillator was employed in checking the angular sensitivity of the neutron scintillator.

tube. Conventional amplifier and scaler arrangements with an integral discriminator permitted the rejection of the relatively small pulses produced by elastically scattered He^3 ions.

In the $Li^7(p,n)Be^7$ calibration, the detector used was a 2-in. diameter 92%-enriched B^{10}-plastic ZnS(Ag) scintillator (Nuclear Enterprises, Ltd., type NE 402), mounted by means of a $\frac{1}{4}$-in. thick conical lucite light pipe to a $1\frac{1}{2}$-in. DuMont 6291 photomultiplier tube, and surrounded by a polyethylene moderator. The geometry of the scintillator assembly is shown in Fig. 2, and its characteristics are discussed below.

The carbon targets used for this part of the experiment were polished pieces of graphite spectroscopic electrodes during the earlier runs, and thick films of carbon, thermally cracked from a methyl iodide atmosphere, for the later runs. The targets used for the $Li^7(p,n)Be^7$ calibration were relatively thick layers of LiF evaporated onto tantalum strips. The excellent gamma-ray rejection of the B^{10}-plastic scintillator permitted the use of these targets with essentially zero background below threshold, despite the strong flux of gamma rays from $F^{19}(p,\alpha\gamma)O^{16}$ reactions. The largest source of background appeared to be (d,n) reactions from residual deuterium in the accelerator. The targets used for the $Au^{197}(d,d)Au^{197}$ elastic scattering were

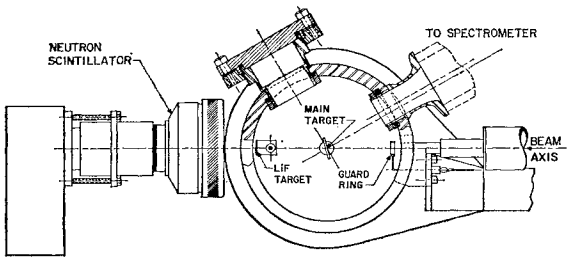

FIG. 3. The experimental arrangement for the measurement of Q_p. The central target rod was used to hold the carbon targets for the $C^{12}(He^3,p)N^{14*}$ reaction and the gold targets for the $Au^{197}(d,d)$-Au^{197} scattering. The auxiliary target rod was used to hold a LiF target for the $Li^7(p,n)Be^7$ threshold determinations.

thick layers of gold evaporated onto glass or polished quartz.

Figure 3 shows the over-all arrangement of target chamber and detectors for this part of the experiment.

3.2. $C^{12}(He^3,n)O^{14}$

The experimental arrangement for this part of the experiment was dictated by the requirements of low background. As there are almost always two or more experiments sharing accelerator time on different experimental stations on the accelerator, neutron background from residual deuterium in the ion source is nearly always a problem. Therefore, to determine the reaction yield, observation was made of the delayed 2.311-MeV N^{14} gamma radiation following the beta decay of the O^{14} produced in the reaction (Fig. 4). This procedure allows all counting to be done with the generator voltage off, thereby eliminating all generator-associated background. In contrast to counting positrons or annihilation radiation, this method also permits

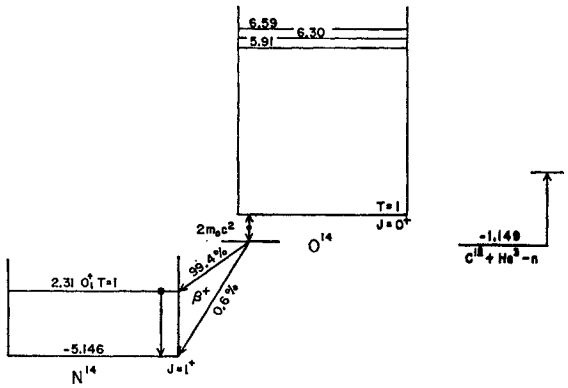

FIG. 4. The energy-level diagram for O^{14}, showing the β^+ transition to the 2.31-MeV, 0^+, $T=1$ first excited state of N^{14}. Energies in MeV.

strong discrimination against the longer half-life positron emitters, C^{11} and N^{13}, which emit no nuclear gamma rays. These two nuclides are produced quite liberally in the reactions $C^{12}(He^3,He^4)C^{11}$ and $C^{12}(d,n)N^{13}$, respectively, the deuterons coming from a small HD^+ contamination in the He^{3+} beam. One can obtain an excellent determination of the small residual background by merely following the 71-sec O^{14} decay for a sufficiently long time.

The arrangement of the apparatus is shown in Fig. 5. The target, either deposited carbon film or polished graphite, was placed in a T-shaped glass target chamber at the end of the extension tube as shown. A 4-in. NaI(Tl) scintillator, mounted on a 5-in. DuMont 6364 photomultiplier tube, was surrounded by a 2-in. thick lead shield and a thick boric acid-loaded plastic neutron shield. This assembly was placed with the face of the crystal about $\frac{3}{4}$ in. from the center line of the target, usually at about 80° in the laboratory, and the whole

front, including the target chamber, shielded with about two inches of lead.

During the $Li^7(p,n)Be^7$ analyzer calibration, the 4-in. scintillator and its shielding assembly were rolled behind a heavy concrete wall to minimize neutron activation of the crystal, and the B^{10} neutron scintillator and moderator assembly described above was placed with the face of the moderator essentially in contact with the target chamber and centered along the beam axis (Fig. 6). Calibration runs were made, as usual, both before and after each threshold run.

A block diagram of the circuitry used for the O^{14} threshold is shown in Fig. 7. Amplified pulses from the photomultiplier were fed to a single-channel differential discriminator, which was set to bracket the photopeak of the 2.31-MeV radiation. The counts from the discriminator output were switched between two alternate scalers by a mechanical timer at 20-sec intervals beginning 4 sec after the end of an activation, which permitted the recording of the counts in one scaler while the other was counting. Timing was checked throughout by counting 120 pulses/sec, derived from

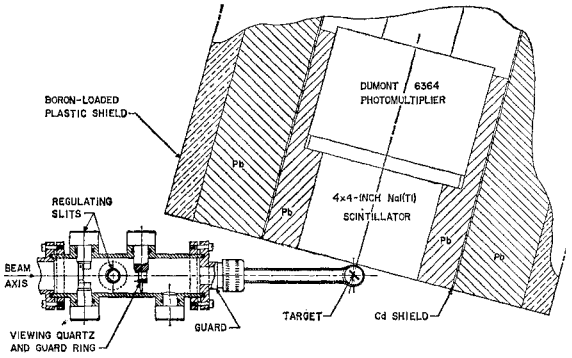

FIG. 5. The experimental arrangement for the $C^{12}(He^3,n)O^{14}$ threshold measurement. Additional shielding surrounding the target chamber is not shown.

the power lines, in secondary channels in the two scalers which were gated in synchronism with the counting periods. Uniform activation of the target, approximately independent of beam-current fluctuations or bombardment time, was obtained by connecting a resistor across the integration capacitor in the target-current integrator to give a time constant equal to the mean life of O^{14}.

The dead time of both scalers was about 10 μsec, which was entirely negligible for the counting rates used in this part of the experiment (about 20 counts/sec maximum).

3.3. O^{14} Half-Life

In the determination of the O^{14} half-life, the considerations of background and other activities discussed above in connection with the $C^{12}(He^3,n)O^{14}$ threshold measurement apply with even greater force, as here

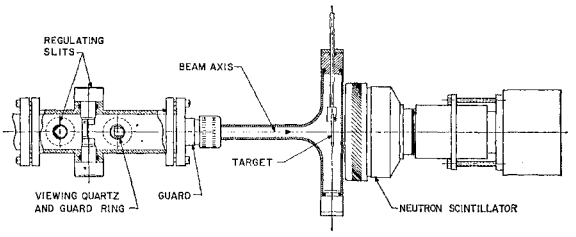

FIG. 6. The arrangement of target and neutron scintillator for the $Li^7(p,n)Be^7$ threshold measurements during the O^{14} threshold experiment.

it becomes essential that one be able to follow the 71-sec decay for several half-lives with minimum interference. For this reason a similar type of experimental arrangement was used. The energy of bombardment was chosen at about 1800 keV to give adequate yield and a reasonable ratio of the $C^{12}(He^3,n)O^{14}$ cross section to the much larger and more rapidly rising cross section[32] for $C^{12}(He^3,He^4)C^{11}$. To achieve maximum O^{14} yield relative to competing reactions, the bombarding time was chosen to be $\cong$100 sec, approximately equal to the mean life. The beam current was the highest value consistent with holding to reasonable levels the loss of O^{14} from the target by overheating or sputtering of the graphite; this value was about 5 μA.

To prevent activation of the NaI crystal by the rather considerable neutron flux produced during a

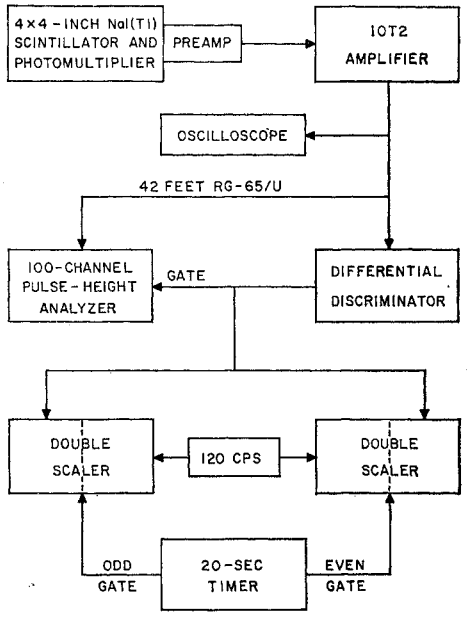

FIG. 7. Block diagram of the counting circuits used in the O^{14} threshold experiment. The 120-cps signal was supplied to the secondary channels of the double scalers to monitor the length of the 20-sec counting intervals.

[32] An exploratory run at about 3.0 MeV produced sufficient positron activity to completely swamp any trace of 2.3-MeV gamma radiation; on the basis of crude estimates of the yield and half-life involved, C^{11} was the most probable source of the activity.

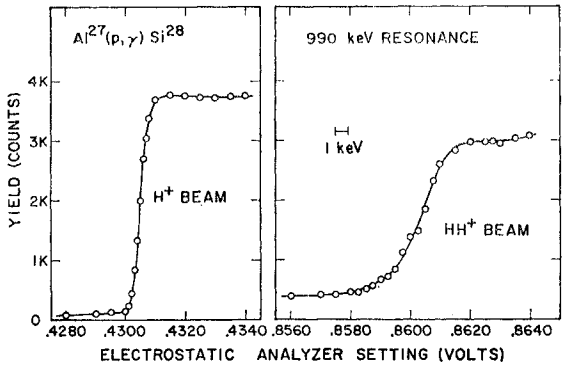

FIG. 8. The $Al^{27}(p,\gamma)Si^{28}$ thick-target resonance yield near 990 keV, as measured with proton and HH^+ molecular-ion beams.

bombardment, the scintillation counter was set up in an adjoining room on the other side of a heavy concrete wall. Polished graphite button targets were activated by He^3 bombardment on the central target rod of the main target chamber (Fig. 3), and then removed and placed in a sealed brass capsule for counting to prevent loss of O^{14} during the counting period. The length of time required to let the target chamber down to atmospheric pressure and transfer the source to its position in front of the counter averaged about one minute. A number of targets were used in rotation to allow time for the background of 10-min N^{13} and 20-min C^{11} to decay between runs with the same target.

A 3×3-in. NaI(Tl) scintillation crystal and photomultiplier assembly was used for this experiment, with shielding very similar to that used in the O^{14} threshold measurements; the only essential difference was that various thicknesses of lead were inserted as an absorber between source and crystal to attenuate preferentially the strong 511-keV annihilation-radiation peak. Without this precaution, it was found that the high counting rate due to this radiation produced a shift in the gain of the photomultiplier as it decayed over the 20-min length of a run, and also raised the problem of superposed "build-up" pulses in the amplifier and discriminator. Absorber thicknesses of 1 and 2 cm were both used, and both were found to be effective; the resulting half-life curves were indistinguishable.

Because of the high initial counting rates involved in this experiment, precautions were necessary to minimize the dead time of the counting system (shown schematically in Fig. 7). For this reason, a Fairstein double-delay-line-clipped nonoverloading amplifier was used, fed from 93-ohm RG-62/U cable driven by a White cathode follower at the photomultiplier. The output from the differential discriminator on the amplifier chassis was used to drive two fast prescalers with a scaling ratio of 8. The outputs of the prescalers were then fed to separate scalers of the ordinary variety.

The linear output of the amplifier was also fed to an oscilloscope and, by way of 42 ft of RG-65/U delay cable, to the signal input of a 100-channel analyzer, which could be gated either by the input pulses or by the output of the differential discriminator. This arrangement permitted examination of the pulse-height spectrum of the amplifier output either *in toto* or in coincidence with those pulses which were actually counted by the scalers. This procedure made it possible to monitor the relationship between the photopeak of the 2.31-MeV radiation and the discriminator levels during the entire course of a run.

The timing for the experiment was provided by gating the two channels of the fast prescaler alternately every 20 sec with the mechanical timer described above. Two additional scalers, also gated alternately by the timer, were used as the time monitor by feeding them with the 10-kc/sec output of a multivibrator frequency divider synchronized with a 100-kc/sec quartz crystal oscillator. This oscillator, in turn, had been checked by comparison with the power line frequency averaged over several days.

The dead time of the counting system was checked with a double-pulse generator and by observation of the waveforms put out by the discriminator and amplifier when fed by an intense source; by either method, it was found to be determined by the 2-μsec length of the delay-line-clipped output of the amplifier. The dead

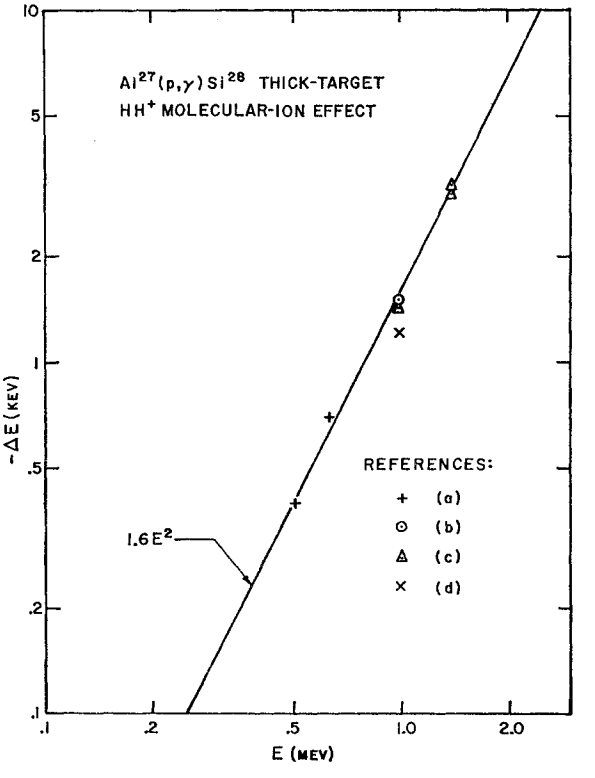

FIG. 9. The difference in position of various resonances in $Al^{27}(p,\gamma)Si^{28}$ as observed with HH^+ molecular ions and as calculated from the resonance energy measured with a proton beam. The sources of the data are (a) Andersen *et al.*,[35] (b) Bondelid *et al.*,[34] (c) the present experiment, and (d) Dahl *et al.*[33] The E^2 dependence is discussed in the text.

time of the fast scalers was less than 1 μsec. The resultant dead-time corrections to the initial counting rate were always less than 1%, and usually of the order of 0.3%.

3.4. Equipment Checks

Electrostatic Analyzer Calibration

As the magnetic spectrometer was known to have a nonlinearity of about 1% over its 10-MeV proton range,[29] the experimental arrangements were chosen so that it was used only at fixed field, as explained above. However, both the proton reaction and the neutron threshold Q values require an extrapolation of the electrostatic-analyzer energy scale from the 1880.7-keV calibration point to the bombarding energies actually used. An experiment to check the linearity of the analyzer was therefore necessary, particularly as the resistors of the voltage measuring dividers were known to have a positive temperature coefficient of about 40 ppm/°C, and the local temperature rise of the encapsulated resistive elements was not known.

An attempt was therefore made to check the linearity of the electrostatic analyzer by comparing apparent energies for the resonances at 991, 1380, and 1387 keV in the $Al^{27}(p,\gamma)Si^{28}$ reaction, as measured with a proton beam, with those obtained using a molecular hydrogen ion beam on thick aluminum targets. This method of checking the analyzer linearity suffers from the serious difficulty that narrow resonances observed with molecular ion beams on thick targets are considerably broadened and shifted to lower energies by the combined effects of the internal motion of the protons within the molecular ion and of the "Coulomb explosion" of the ion after its remaining electron is stripped off in the target.[33] The detailed shape of the resulting asymmetrically broadened resonance (Fig. 8) and the apparent shift produced depend on the interactions of the rate of expansion of the ion in its explosion, the rate of energy loss of the protons in the target material, and the beam energy resolution, all of which are functions of bombarding energy, and in addition on the internal motion of the ion. Figure 9 shows the apparent resonance shifts observed in the present work and by other experimenters.[34,35] Calculations based on a simplified model of the Coulomb explosion effect indicate that the E^2 dependence of the shift displayed in Fig. 9 is consistent with the model, providing justification for the extrapolation of the lower energy data to the vicinity of the 1380-keV resonances. We conclude that there is no evidence for a shift in the calibration of our electrostatic analyzer with energy within the limits of accuracy of the measurement. At the beam energy resolution used in the present experiment ($\approx 0.1\%$) errors caused by variations in the shapes of the resonance due to the Lewis effect[36] would be negligible.

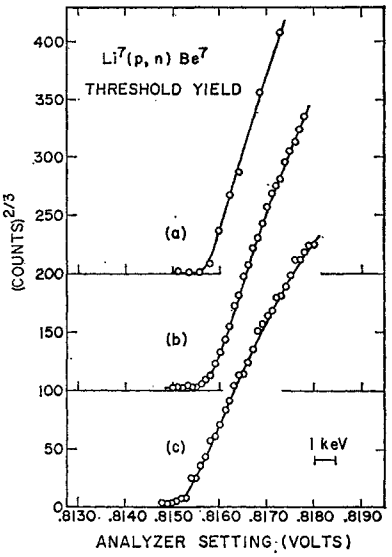

FIG. 10. Typical $\frac{3}{2}$-power plots of the $Li^7(p,n)Be^7$ neutron yield as a function of proton energy. The variations in the potentiometer readings at the neutron threshold are due to the different geometrical alignments of the electrostatic analyzer used in various parts of the experiment. Curves (a) and (b) have been displaced upwards for display purposes.

An experiment is currently in progress to check the analyzer linearity by comparing the analyzer settings which correspond to He^+ and He^{++} ions of the same energy, an experiment which is free from the molecular ion complications.

Neutron Scintillation Counter

The recommended procedure for $Li^7(p,n)Be^7$ neutron threshold experiments requires the extrapolation to zero yield of the $\frac{2}{3}$ power of the neutron yield, in order to linearize the expected $\frac{3}{2}$-power energy dependence of the thick-target neutron yield for an s-wave neutron threshold. It is assumed that the solid angle of the neutron counter is sufficiently large to include the entire cone of emitted neutrons for a range of several keV above threshold, and that the detector response is independent of neutron energy. In order to check the counter solid angle, the variable-angle target chamber and neutron counter were arranged as in Fig. 2, and the incoming beam energy was set about 0.7 keV above threshold. This confines the neutrons to a cone of half-angle $\approx 8°$. By rotating the neutron counter through the narrow cone of neutrons, it was found that

[33] P. F. Dahl, D. G. Costello, and W. L. Walters, Nuclear Phys. **21**, 106 (1960); D. G. Costello, W. L. Walters, and R. G. Herb, Bull. Am. Phys. Soc. **6**, 250 (1961).

[34] R. O. Bondelid, J. W. Butler, and C. A. Kennedy, Bull. Am. Phys. Soc. **2**, 381 (1957); R. O. Bondelid and C. A. Kennedy, U. S. Naval Research Laboratory Report NRL-5083, 1958 (unpublished).

[35] S. L. Anderson, K. Gjötterud, T. Holtebekk, and O. Lönsjö, Nuclear Phys. **7**, 384 (1958).

[36] W. L. Walters, D. G. Costello, J. G. Skofronick, D. W. Palmer, W. E. Kane, and R. G. Herb, Phys. Rev. Letters **7**, 284 (1961).

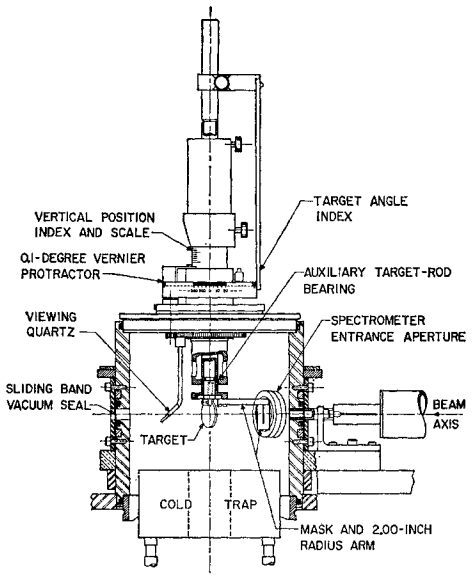

FIG. 11. The experimental arrangement used to measure the angle between the incoming beam and the magnetic spectrometer entrance aperture. The mask shown contains a 0.040-in. vertical split aperture at 2.00-in. radius from the target axis; the angular position of the slit may be read on the vernier protractor.

the counter sensitivity was approximately uniform over a cone of half-angle 50°. This was more than adequate for the present experiment, since a cone angle of this size corresponds to a bombarding energy 22 keV above threshold.

The excellent linearity of the $\frac{2}{3}$-power plots of the neutron yield over the first 5 keV above threshold, shown in Fig. 10, is probably fortuitous, since calculations based on detailed investigations of the neutron yield[37,38] suggest that the thick target yield should fall below a $\frac{3}{2}$-power energy dependence. It may be that the expected decrease in yield is compensated by an improved detection efficiency for the neutrons which are emitted in a backward direction in the center-of-mass system, and hence have lower laboratory energies as the beam energy is raised. In any case, small variations in the shape of the yield vs energy curve have little effect on the extrapolation to threshold providing the background yield is small compared to the yield from the reaction.

Angular Position of the Magnetic Spectrometer

From the kinematics of the $C^{12}(He^3,p)N^{14*}$ reaction and the associated calibrations, it may be shown that $\partial Q_p/\partial\theta = 6$ keV/deg. It is therefore important to determine the angular position of the spectrometer with a precision of the order of a few hundredths of a degree. The angle between the entering beam and the centroid of the solid angle of acceptance of the magnetic spectrometer was measured for each series of runs on the $C^{12}(He^3,p)$ reaction with the experimental arrangement shown in Fig. 11. The yield of protons elastically scattered from a thick gold target was obtained as a function of the position of a 0.040-in. vertical slit at the end of a 2.00-in. radius arm. The slit was swept across both the beam and the spectrometer aperture while the target position was held fixed. The position of the slit was read on the vernier protractor shown in Fig. 11, which could be set to about 0.05° accuracy. A plot of the resulting yield vs slit angle is given in Fig. 12 for Au^{197}-$(p,p)Au^{197}$ scattering, and also for $Au^{197}(He^{4+},He^{4++})$-$Au^{197}$ scattering, with a bombarding energy of 1.90 MeV and the same laboratory angle of approximately 150°.

The angles of the centroids of the yield distributions across the beam and across the spectrometer aperture were then calculated, and their difference taken as the actual angle of observation in the laboratory. The He^4 scattering, as it involves incoming and outgoing particles of widely differing magnetic rigidity, was used here to help estimate the effects of stray magnetic fields from the spectrometer on the entrance and exit angles. By subtracting the proton results and the He^4 results, the entrance angles were found to differ by 0.06°, the exit angles by 0.04°, and their difference θ_{lab} by 0.03°. These results also give some indication of the reproducibility of this technique of measuring the angle.

The values resulting from this measurement must, in principle, be corrected for the variation of the Rutherford scattering yield across the $3\frac{1}{2}$°-wide aperture of the spectrometer, which produces a small systematic shift in the location of the centroid of the yield distribution. However, calculation shows the resultant correction to be only of the order of 0.007°, and hence negligible.

Microscopic examination of the motions of the slit and target-holder assembly disclosed the existence of a geometrical eccentricity in the apparatus which could result in an error in the measured exit angle of slightly over 0.05° in the worst orientation of the system. The

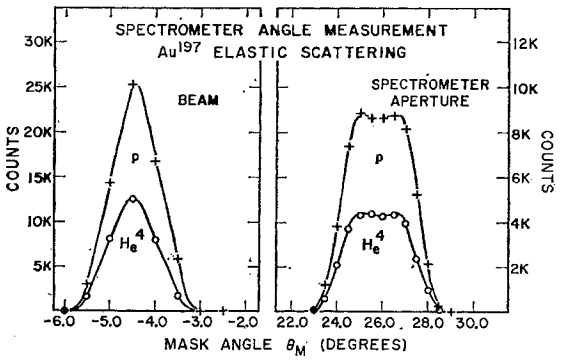

FIG. 12. The yields of $Au^{197}(p,p)Au^{197}$ and $Au^{197}(He^{4+},He^{4++})$ Au^{197} elastic scattering vs slit angle as the mask is moved across the incoming beam and the spectrometer aperture in the experimental arrangement of Fig. 11.

[37] H. W. Newson, R. M. Williamson, K. W. Jones, J. H. Gibbons, and H. Marshak, Phys. Rev. **108**, 1294 (1957).
[38] R. L. Macklin and J. H. Gibbons, Phys. Rev. **109**, 105 (1958).

contribution of this effect to the standard deviation of the measurement was therefore taken as $\pm 0.05°$. This was combined with an additional protractor calibration error of $\pm 0.06°$, which was determined by comparing the protractor used in the spectrometer angle experiment with a precision protractor. The combined error from the protractor calibration and target eccentricity errors is then $\pm 0.08°$.

Corrections Resulting from Finite Spectrometer Resolutions

It can be shown[30] that there are also small corrections to the apparent position of the midpoint of the thick target yield step of the $C^{12}(He^3,p)N^{14*}$ reaction due to the variations of the reaction yield over the spectrometer resolution windows in energy and angle. Using measured values of these variations at the energy and angle used in the experiment, calculation shows that the resultant correction to Q_p is about 0.004%. As this small value should be further reduced by the fact that we fitted the rising faces of our yield profiles with straight lines rather than the curves for which the correction was calculated, this effect was also neglected.

4. EXPERIMENTAL RESULTS AND ANALYSIS OF DATA

4.1. $C^{12}(He^3,p)N^{14*}$ (2.311-MeV State)

Typical profiles resulting from the $C^{12}(He^3,p)N^{14*}$ experiment are shown in Figs. 13, 14, and 10(b). Figure 13 shows the yield of protons of energy 3.633 MeV at approximately 150° laboratory angle from the $C^{12}(He^3,p)N^{14*}$ reaction near a bombarding He^3 energy of 2.69 MeV, and Fig. 14 shows the deuteron yield from $Au^{197}(d,d)Au^{197}$ elastic scattering with the same spectrometer field and angle, near a bombarding energy of 1.88 MeV. Figure 10(b) shows the $Li^7(p,n)Be^7$ neutron threshold, the primary calibration point, as taken with the experimental arrangement for this reaction (Fig. 3).

TABLE I. Errors contributing to the standard deviation of Q_p (in keV).[a]

Source	Set I		Set II
Angle measurement ($\pm 0.03°$)	± 0.18		± 0.18
Analyzer linearity measurement	± 0.76		± 0.16
Dispersion of measured values	± 0.36		± 0.28
Resultant standard deviations	± 0.86		± 0.37
Resultant weights	1.0		5.4
Standard deviation of weighted mean		± 0.34	
External error		± 0.44	
Protractor calibration, etc. ($\pm 0.08°$)		± 0.48	
Energy scale uncertainty		± 0.53	
Uncertainty in form of analyzer correction		± 0.50	
Final standard deviation of Q_p		± 1.03	

[a] The various sources of error contributing to the standard deviation of Q_p are given in terms of their effects on Q_p for two sets of seven runs each.

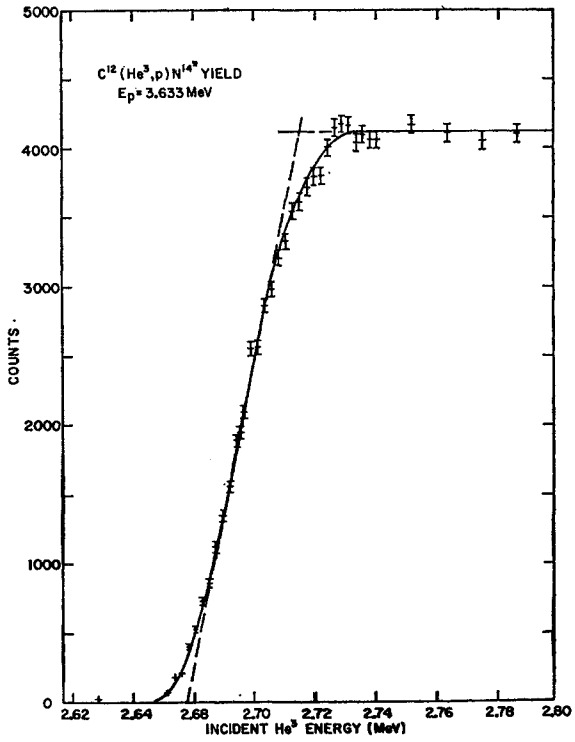

FIG. 13. The yield of the reaction $C^{12}(He^3,p)N^{14*}$ (2.311-MeV state) as a function of incident energy with the magnetic spectrometer set to accept 3.633-MeV protons at $\theta_{lab}=150°$.

Values were taken from the two spectrometer profiles by drawing a straight line through the points on the face of each profile and reading the electrostatic analyzer setting corresponding to the point on this line midway between background and maximum yield levels (Figs. 13 and 14). The neutron threshold was obtained from the usual linear extrapolation of the $\frac{2}{3}$ power of the yield above background.

Sixteen runs of the proton reaction were made, and the resultant values of Q_p were divided into two groups of eight, according to whether the corresponding run was made before or after the installation of a heat exchanger on the electrostatic analyzer power supply. This installation made a noticeable improvement in the reproducibility of the results, and eliminated a small correction for thermal drift which had been necessary previously. Because of this change and the fact that the two sets of data were taken with separate and independent measurements of the spectrometer angle, a separate analysis of the errors in each of the two sets was made. These analyses are summarized for the two sets, labeled I and II, respectively, in Table I.

The values shown in Table I are standard deviations given in terms of the effect of the uncertainty in question on the value of Q_p in keV. The errors which affect each set of data independently are the angle-measurement reproducibility, estimated from the experiment described above where the same angle was

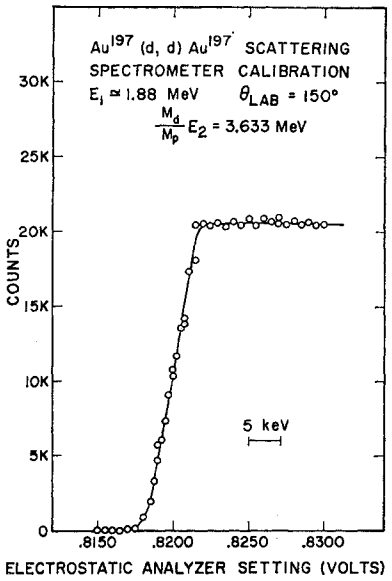

FIG. 14. The yield vs incident energy of the $Au^{197}(d,d)Au^{197}$ elastic scattering used to calibrate the magnetic spectrometer against the electrostatic analyzer.

measured twice using protons and He^4, respectively, the estimated experimental error in the analyzer linearity-check experiment, and the experimental error in performing the actual $C^{12}(He^3,p)N^{14*}$ reaction experiment. The analyzer linearity error quoted for Set I is the result of three runs of the reaction $Al^{27}(p,\gamma)Si^{28}$, and shows the effects of thermal drifts still present in the electrostatic analyzer supply at that time. The value for Set II illustrates the improvement in stability of calibration resulting from the stabilization of the analyzer power supply temperature.

One value of Q_p in each set was found to be far outside the limits of the others, and was accordingly discarded. The dispersion of the remaining seven points in each set was then used to calculate the statistical standard deviation of the mean of the set. Combining the experimental errors above with the standard deviations of the means, we arrive at standard deviations for each set, the weighting for a weighted mean of the two sets, and the standard deviation of that mean. With a weighting in the ratio of 1:5.4 favoring Set II, this internal standard deviation is ± 0.34 keV. The external standard deviation calculated from the dispersion of the means of the two sets is ± 0.44 keV, in reasonable agreement.

To arrive at the final standard deviation for Q_p, we must combine this last value with the errors which affect the two sets of data coherently. These include the error arising from the uncertainty in observation angle due to protractor calibration errors and target eccentricities, estimated at $\pm 0.08°$, the uncertainty due to the error in the adopted value of the $Li^7(p,n)Be^7$ threshold, 1880.7 ± 0.4 keV, and an uncertainty resulting from the possible deviation of the molecular ion effect from its assumed E^2 dependence in the analyzer linearity-check experiment. The latter was estimated as ± 0.5 keV by trying various assumed forms for the energy dependence. The final result is

$$Q_p = 2468.4 \pm 1.0 \text{ keV}.$$

4.2. $C^{12}(He^3,n)O^{14}$

At intervals during the course of each of the two runs made of the O^{14} threshold measurement, the O^{14} activity of the target was allowed to decay to a level well below background. Logarithmic plots of the 2.31-MeV gamma-ray yield as a function of time following activation were then used to determine the magnitude and time dependence of the background; at no time during either run was there any evidence of

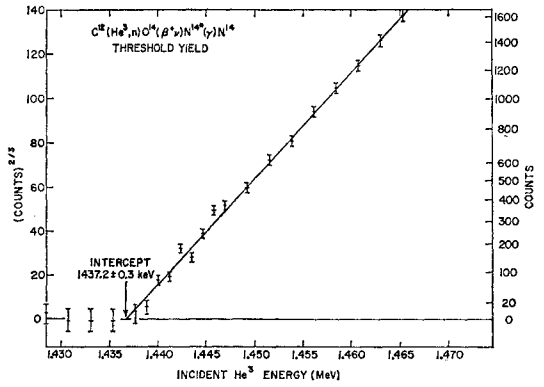

FIG. 15. Threshold yield curve for $C^{12}(He^3,n)O^{14}$. The $\frac{2}{3}$ power of the yield of 2.31-MeV gamma rays following the O^{14} decay is plotted versus incident He^3 energy. The straight line is a least-squares fit.

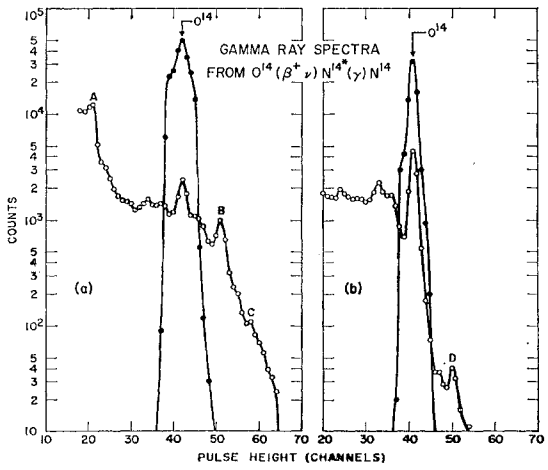

FIG. 16. Gamma-ray spectra taken in the O^{14} half-life measurement. The spectra selected by the differential discriminator are multiplied by ten and superimposed on the raw pulse-height spectra. The curves (a) were obtained without absorber and the curves (b) with a 2-cm lead absorber in front of the scintillation counter. The peak marked A is due to pileup of two annihilation quanta, and the peak C is due to addition of two annihilation quanta to the 2.31-MeV gamma-ray energy. These peaks are removed by the absorber. Peaks B and D are due to the superposition of one coincident annihilation quantum on the 2.31-MeV gamma ray.

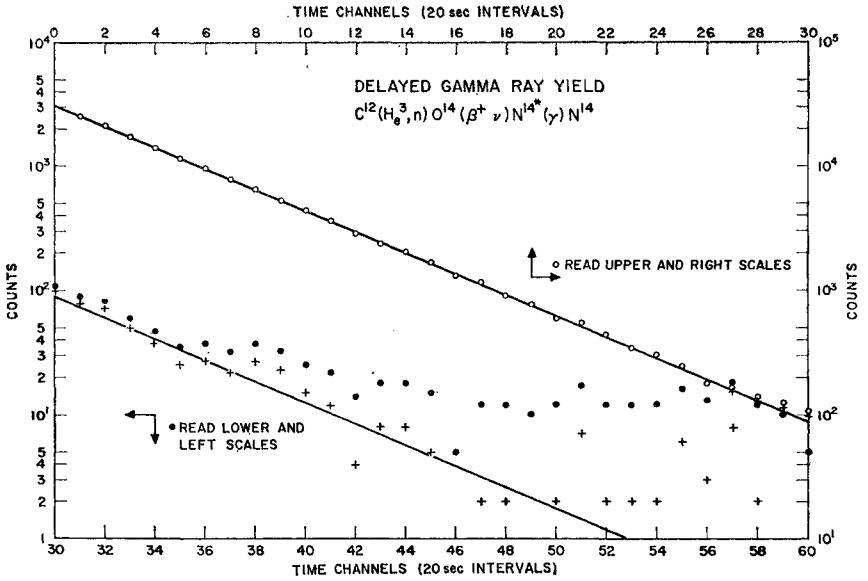

FIG. 17. The yield of delayed 2.31-MeV gamma rays from the decay of O^{14} versus time. A small dead-time correction has already been made to the first few points. The crosses show the effect of subtracting a constant background of 10 counts per 20-sec time channel. The line shown is a least-squares fit.

longer half-life contaminations such as C^{11} or N^{13}. The yield curves were also examined for evidence of nonlinearity in their initial portions. No such distortions were found, indicating that such effects as loss of O^{14} from the target and short half-life contaminations were small, and confirming the evidence of direct measurements that the counter dead times were negligible.

Figure 15 shows the $\frac{2}{3}$ power of the delayed gamma-ray yield in excess of background plotted vs energy of bombardment near threshold for one run. The value plotted is the sum of the counts for the first 120 sec of each decay curve, corrected for background and for the remaining activity from the previous bombardment. In order to minimize this last correction, the readings were taken in order of increasing bombarding energy. This curve is a striking example of the expected s-wave neutron threshold behavior. The points where the yield was negative after background subtraction are plotted below zero on the $\frac{2}{3}$-power plot in the interests of better display.

Least-squares fitted intercepts were calculated for both runs using uniform weighting of the points. Both of these fittings gave a standard deviation of ± 0.2 keV in the value of Q_n; however, the external error calculated from the spread of the two values was ± 0.5 keV in Q_n. Combining this value with an almost negligible contribution of ± 0.1 keV from the linearity measurements on the electrostatic analyzer, and with the uncertainty in the $Li^7(p,n)Be^7$ energy scale, we arrive at the final values

$$Q_n = -1148.8 \pm 0.6 \text{ keV},$$
$$E_{th} = 1437.5 \pm 0.7 \text{ keV}.$$

4.3. O^{14} Half-Life

The results of the O^{14} half-life experiment are illustrated in Figs. 16 and 17. Figure 16 is a semilogarithmic plot of typical delayed gamma-ray pulse-height spectra taken during this experiment, showing (a) the full spectrum of the target without the lead absorber which was used during the actual measurement, and (b) the spectrum as run, with a 2-cm Pb absorber between the O^{14} source and the scintillator to attenuate the annihilation radiation. In both cases the spectrum of the pulses coincident with the output of the differential discriminator is shown superimposed on the full spectrum. In the spectra without the lead absorber, it is interesting to note that the annihilation radiation is sufficiently intense to produce the peak at point A by superposing two annihilation quanta, and the peaks at B and C by superposing one and two annihilation quanta, respectively, on the 2.31-MeV gamma ray. In contrast, with the absorber in place, the summing peak at D is greatly reduced, and the resolution for the N^{14} gamma ray is considerably improved. The 2-cm absorber was used for four of the five runs made of this experiment; the fifth, using a 1-cm absorber, gave very similar spectra and a decay curve indistinguishable in shape from the other runs. Figure 17 shows a semilogarithmic plot of the yield from the discriminator vs time after correction for dead time. The result of subtracting a constant background is also shown.

The five runs were analyzed by least-squares fittings of straight lines to the natural logarithms of the counts, corrected for dead time and background, taken as a function of time in 20-sec counting intervals. The logarithmic count for each time channel was weighted according to the square of the corrected counts divided by the raw counts to take into account the effect on the standard deviation of the addition of the relatively well-known dead time and background corrections to the raw counts.

The decay curves for the various runs were investigated for time-dependent background, faults in

TABLE II. Summary of experimental results.

$C^{12}(He^3,p)N^{14*}$	$Q_p=2468.4\pm1.0$ keV
$C^{12}(He^3,n)O^{14}$	$Q_n=-1148.8\pm0.6$ keV
	$E_{th}=1437.5\pm0.7$ keV
End-point energy	$E_{max}(\beta^+)=1812.6\pm1.4$ keV
	$W_{max}(\beta^+)=2323.6\pm1.4$ keV
f value	$f=42.97\pm0.13$
Half-life of O^{14}	$t=71.00\pm0.13$ sec
Half-life corrected for ground-state branch	$t^*=71.43\pm0.15$ sec
Uncorrected ft value	$ft^*=3069\pm12$ sec
Mean half-life[a]	$t^*=71.36\pm0.09$ sec
Uncorrected ft value[a]	$ft^*=3066\pm10$ sec

[a] Half-life measurements of the present experiment and that of Hendrie and Gerhart from reference 40 weighted inversely as the quoted error.

the dead-time correction, and other possible distortion mechanisms by comparing half-lives fitted to various portions of each curve, and also by inspection of the time dependence of the background remaining after subtracting the least-squares fitted decay from the raw counts plus dead-time correction. No evidence of such distortion of the decay curve was found.

The final weighted average of the five runs of the O^{14} half-life experiment is $t=71.00\pm0.13$ sec, where the standard deviation quoted is the external standard deviation from the scatter of the values from the five runs. The internal standard deviation was ±0.09 sec.

The above value differs slightly from the value 71.1 ± 0.2 sec quoted in the preliminary report[21] of this experiment as a result of the inclusion of two additional runs for which the analysis was not completed in time for the earlier publication.

4.4. Summary of Results: The ft Value of the Transition

Table II summarizes the various results of the experiment. The value of $E_{max}(\beta^+)=1812.6\pm1.4$ keV was calculated from Eq. (3). The value of f was found by numerical integration from the National Bureau of Standards' *Tables for the Analysis of Beta Spectra.*[39] A small correction (-0.065%) was applied to the result to take into account the more recent value[23] of the electron mass ($m_ec^2=0.510976$ MeV).

Our value for the half-life of O^{14}, $t=71.00\pm0.13$ sec, when corrected for the ground-state branch[25] of the decay, $(0.6\pm0.1)\%$, gives $t^*=71.43\pm0.15$ sec for the half-life of the transition to the N^{14*} excited state. This gives an uncorrected ft value of 3069 ± 12 sec. This half-life has also been carefully measured recently by Hendrie and Gerhart,[40] who give the weighted mean of 40 runs as $t=70.91\pm0.04$ sec, in quite satisfactory agreement. This leads to values of the partial half-life and ft value $t^*=71.34\pm0.08$ sec and $ft=3065\pm10$ sec, respectively, using the f value from Table II. If the two total half-life measurements are averaged with weights inversely as the quoted standard deviations, we find $t^*=71.36\pm0.09$ sec and $ft=3066\pm10$ sec.

5. DISCUSSION AND CONCLUSIONS

5.1. Comparison with Previous Results

In order to compare the Q value resulting from the $C^{12}(He^3,p)N^{14*}$ experiment with the values calculated from the mass tables, we use the result of Sanders[41] for the excitation of N^{14*}. Corrected for the new value of the $Li^7(p,n)Be^7$ threshold,[26] this is 2311.4 ± 1.2 keV, which yields a Q value for the $C^{12}(He^3,p)N^{14}$ ground-state reaction of 4779.8 ± 1.5 keV when combined with our result. This is in good agreement with the value 4778.6 keV calculated from the mass tables of Everling *et al.*,[22] but definitely disagrees with the value 4767.8 ± 3.9 keV from the older tables of Mattauch *et al.*[15]

The agreement of our $C^{12}(He^3,p)N^{14*}$ Q value with the later mass tables is very satisfactory, but as no direct experimental data on this Q value contributed to the mass-table value, this agreement represents only an indirect confirmation of our value. It is therefore highly desirable that additional direct measurements of the $C^{12}(He^3,p)N^{14*}$ Q value be made by other laboratories.

The predictions of the mass tables for the Q value of the $C^{12}(He^3,n)O^{14}$ reaction are not nearly as precise; the tables of Mattauch *et al.*[15] give $Q_n=-1166\pm39$ keV, while those of Everling *et al.*[22] predict $Q_n=-1152\pm5$ keV. From Table II, our experimental value is $Q_n=-1148.8\pm0.6$ keV, consistent with either set of tables.

The experimental situation for the $C^{12}(He^3,n)O^{14}$ threshold is considerably better. Our value for $Q_n=-1148.8\pm0.6$ keV differs but slightly from the latest of the series of measurements made by the NRL group,[17–19] which gives $Q_n=-1147.7\pm0.7$ keV. Both of these measurements disagree with the older measurements of Bromley *et al.*[14] $Q_n=-1158.5\pm3$ keV.

Aside from direct beta-spectrometer measurements, there exist at present no other determinations of the O^{14} beta-decay end-point energy which have not necessarily depended on the mass tables for a calculated value of Q_p. We can therefore only compare the result of the present experiment $E_{max}(\beta^+)=1812.6\pm1.4$ keV with the spectrum measurements of Penning and Schmidt,[13] and of Gerhart[12]; Gerhart gives $E_{max}(\beta^+)=1835\pm8$ keV, in rather poor agreement with the present value.

The half-life of the transition has a considerable experimental history.[12,25,40,42] The earlier experiments, however, seem to have suffered from the ease with which longer-lived positron emitters are produced

[39] "Tables for the Analysis of Beta Spectra," *National Bureau of Standards Applied Mathematics Series No. 13* (U. S. Government Printing Office, Washington, D. C., 1952).

[40] D. L. Hendrie and J. B. Gerhart, Phys. Rev. **121**, 846 (1961).

[41] R. M. Sanders, Phys. Rev. **104**, 1434 (1956).

[42] R. Sherr, H. R. Muether, and M. G. White, Phys. Rev. **75**, 282 (1949).

TABLE III. Effect of various theoretical corrections on the comparison of G_V and G_μ.

	Uncorrected	Nonradiative[a] corrections	Nonradiative[b] and radiative	Nonradiative[c] and radiative	Units
O^{14}		+0.265	+1.7[g]	−1.03[d]	% of ft
ft	3066±10[f]	3074	3126	3043	sec
G_V	1.4164±0.0022	1.4145	1.4025	1.4218	$\times 10^{-49}$ erg-cm^3
	1.0131±0.0016	1.0118	1.0031	1.0170	$\times 10^{-5}/M_p^2$ ($\hbar=c=1$)
Muon			−0.42[d]	−1.32[d]	% of τ_μ
τ_μ	2.210 ±0.003		2.201	2.181	μsec
G_μ	1.4282±0.0011		1.4312	1.4377	$\times 10^{-49}$ erg-cm^3
	1.0215±0.0008		1.0237	1.0284	$\times 10^{-5}/M_p^2$ ($\hbar=c=1$)
$(G_\mu-G_V)/G_\mu$	0.8 ±0.2[e]	1.0	2.0	1.1	%

[a] Electron screening and nuclear electromagnetic form factor effects, K-capture competition and second-forbidden matrix-element corrections from reference 6.
[b] Radiative corrections from reference 5.
[c] Radiative corrections from reference 6.
[d] Radiative corrections only.
[e] Averaging in the recent muon lifetime measurement of R. A. Lundy [Phys. Rev. **125**, 1686 (1962)] $\tau_\mu=2.203\pm0.004$ μsec, increases $(G_\mu-G_V)/G_\mu$ by 0.1%.
[f] It has been pointed out (J. M. Pearson, private communication) that the second term in the usual expansion of the Fermi function is not entirely negligible at the present level of precision. A calculation of this term indicates that one should reduce the O^{14} ft value by about 7 sec.
[g] S. M. Berman and A. Sirlin (to be published) have recently re-examined the radiative corrections to the O^{14} ft value, with the result (+1.7 ±1.0) percent, and have placed the correction to the muon lifetime on a more rigorous basis.

along with O^{14}. The result of the present experiment, $t=71.00\pm0.13$ sec, disagrees with Gerhart's earlier result,[12] $t=72.1\pm0.4$ sec, but is in good agreement with the recent measurement of Hendrie and Gerhart[40] $t=70.91\pm0.04$ sec.

5.2. Theoretical Corrections and the Value of the Fermi Coupling Constant

Before calculating G_V, a number of theoretical corrections must be made to the uncorrected O^{14} ft value above, 3066±10 sec. The first group of corrections, relatively free of theoretical uncertainty, are those due to the effects of nuclear electromagnetic form factors and electron screening on the electronic wave functions in the beta decay, and to the effects of competition from K-electron capture. As listed by Durand *et al.*,[6] these effects result in a total correction of +0.289% to f. For reference, these will be termed electronic corrections.

The remaining corrections necessary are the radiative or electromagnetic corrections to both the muon decay and the O^{14} decay, and a series of corrections to the nuclear matrix element of the O^{14} decay.[6,43,44] These remaining corrections are all subject to varying amounts of theoretical uncertainty. In view of this uncertainty, the effects of these various corrections will be shown in detail in Table III.

The first column in Table III shows the uncorrected results of the O^{14} ft value measurement. The Fermi coupling constant G_V is calculated from the relation[45]

$$G_V^2 ft=\pi^3\hbar^7(\ln 2)/m_e^5c^4.$$

G_V is also given in theoretical units ($\hbar=c=1$) by multiplying by $M_p^2c/\hbar^3=0.7153\times10^{44}$ erg^{-1} cm^{-3}. The corresponding relation for the coupling constant in muon decay is

$$G_\mu^2\tau_\mu=192\pi^3\hbar^7/m_\mu^5c^4.$$

Recent experimental measurements of the muon mean life have given $\tau_\mu=2.211\pm0.003$ μsec[7] and $\tau_\mu=2.208\pm0.004$ μsec,[8] which average to $\tau_\mu=2.210\pm0.003$ μsec. The three recent muon mass measurements are those of Lathrop *et al.*[9] [$m_\mu=(206.76\pm0.03)m_e$], Devons *et al.*[10] [$m_\mu=(206.78\pm0.03)m_e$], and of Charpak *et al.*[11] [$m_\mu=(206.77\pm0.01)m_e$]. The first two of these mass measurements are critical μ-mesic x-ray absorption experiments of the type described by Koslov, Fitch, and Rainwater.[46] The third value results from a verification of the quantum electrodynamic g factor for the muon by a technique similar to the recent electron experiment of Schupp, Pidd, and Crane.[47] This result was combined with the muon magnetic moment measurement of Garwin *et al.*[48] to get the muon mass. It is worth noting that the relations governing the various types of magnetic moment and g factor experiments are derived from the classical covariant equations of motion in a brief but comprehensive note by Bargman, Michel, and Telegdi.[49]

Inserting the average muon mass and mean life in the relation for G_μ, we find $G_\mu=(1.4282\pm0.0011)\times10^{-49}$ erg-cm^3. The percentage discrepancy between G_μ and G_V is then calculated, yielding (0.8±0.2)%.

The second column of Table III includes the +0.289% electronic corrections mentioned above, and in addition, the very small correction of −0.024% given by Durand *et al.*[6] for the effects of second-forbidden matrix elements.

[43] W. M. MacDonald, Phys. Rev. **110**, 1420 (1958).
[44] H. A. Weidenmüller, (private communication) [Phys. Rev. (to be published)].
[45] E. J. Konopinski, Ann. Rev. Nuclear Sci. **9**, 99 (1959).
[46] S. Koslov, V. Fitch, and J. Rainwater, Phys. Rev. **95**, 291 (1954).
[47] A. A. Schupp, R. W. Pidd, and H. R. Crane, Phys. Rev. **121**, 1 (1961).
[48] R. L. Garwin, D. P. Hutchison, S. Penman, and G. Shapiro, Phys. Rev. **118**, 271 (1960).
[49] V. Bargmann, L. Michel, and V. L. Telegdi, Phys. Rev. Letters **2**, 435 (1959).

In principle, the Coulomb corrections to the nuclear matrix element should be made at this point. The recent work of Weidenmüller,[44] however, indicates that the magnitude of the Coulomb corrections is at present very uncertain. We will therefore exclude Coulomb corrections from Table III.

The third and fourth columns of the table include, in addition, the radiative corrections to both the O^{14} *ft* value and the muon mean life, as calculated by Kinoshita and Sirlin,[5] and Durand *et al.*,[6] respectively. It should be pointed out that the calculations of Durand *et al.* are based on a quite different theoretical approach from that of Kinoshita and Sirlin, resulting in a different definition of the coupling constant. Hence, neither the values of G_V nor the values of the corrections are expected to be comparable in the two cases. The O^{14} radiative correction of Kinoshita and Sirlin includes a contribution from the anomalous magnetic moments of the neutron and proton which they have estimated at $+0.2\%$ from the work of Berman.[4] Thus we see from Table III that the remaining discrepancy between G_μ and G_V in the absence of Coulomb effects is 2.0% if one uses the radiative corrections of Kinoshita and Sirlin[5] or 1.1% if one uses the corrections of Durand *et al.*[6]

5.3. Theoretical Considerations and Conclusions

The above calculations have been made on the assumption that the Fermi interaction is a contact interaction between the four fermions involved in the decay. It is interesting to note the effects of the suggestion, which has recently attracted some attention,[1,50–52] that the interaction in fact involves two vertices connected by the exchange of an intermediate heavy charged vector meson. Lee and Yang[50] have calculated this nonlocal effect on the decay rate of the muon, finding that[53] $W=W_0[1+0.6(m_\mu/m_B)^2]$, where W_0 is the decay rate for the contact interaction, and m_μ and m_B are the masses of the muon and the intermediate meson, respectively. Due to the much lower momenta involved, the effect on nuclear beta decay is completely negligible. As the mass m_B must be at least that of the K meson to forbid the rapid decay of the K meson into the intermediate meson, the maximum possible correction to the muon lifetime from direct intermediate meson effects must be very close to $+0.6(m_\mu/m_K)^2 = +2.8\%$, yielding a correction to G_μ of -1.4%. It should be noted that recent measurements of the Michel parameter ρ for the muon decay spectrum[54] seem to indicate that m_B may be of the same order as m_K.

Evidently, the existence of the intermediate vector meson may have a significant effect on the agreement between G_μ and G_V. Unfortunately, its existence may also invalidate present calculations of the radiative corrections to muon decay, thus introducing further theoretical uncertainty.

An alternative explanation of the apparent discrepancy between G_V and G_μ has been suggested by Blin-Stoyle and LeTourneux.[55] These authors show that the expected small charge dependence of the internucleon potential due to the difference in mass of the charged and neutral pions, and due to different radiative corrections to the nucleon-pion vertices, may reduce the matrix element in the O^{14} beta decay by a sufficient amount to remove the apparent discrepancy.

A third possible explanation of the apparent discrepancy between G_V and G_μ arises from uncertainties in the calculation of the Coulomb corrections to the nuclear matrix element of the decay. The value -0.35% used by Durand *et al.*[6] for this correction was taken from the upper limit calculated by MacDonald.[43] A more elaborate calculation of this effect, based on similar premises, has recently been carried out by Weidenmüller.[44] Using pure $1p$-shell states for the unperturbed wave functions, and properly antisymmetrizing the resulting wave functions, he finds an upper limit of about -0.1% on very conservative assumptions as to the correct energy-level spacing. He points out, however, that the calculation would be invalidated by the presence of appreciable configuration mixing of higher states into the $1p$-shell states involved in the decay, a possibility for which there may be some evidence.[56] In this eventuality it is easily conceivable that strong enhancement of the Coulomb effects could occur; a 1% or 2% effect cannot be excluded.

In conclusion, since the experimentally determined discrepancy between G_V and G_μ is less than the uncertainty in the theoretical calculations of the necessary corrections to G_V and G_μ, the present experiment must be interpreted as supporting the conserved-vector-current hypothesis.

ACKNOWLEDGMENTS

The authors take pleasure in acknowledging their indebtedness to Professor R. F. Christy, Professor R. P. Feynman, Professor M. Gell-Mann, Professor H. A. Weidenmüller, and Dr. J. C. Pati for many valuable theoretical discussions.

[50] T. D. Lee and C. N. Yang, Phys. Rev. **108**, 1611 (1957); further references are given in the review by L. Okun', Ann. Rev. Nuclear Sci. **9**, 61 (1959).

[51] S. Oneda and J. C. Pati, Phys. Rev. Letters **2**, 125 (1959).

[52] J. D. Childress, Phys. Rev. **123**, 1729 (1961).

[53] See also Oneda and Pati (see reference 51). Childress (see reference 52) disagrees with this value. It must also be pointed out that Hendrie and Gerhart (reference 40) are not correctly quoted in reference 52.

[54] R. J. Plano, Phys. Rev. **119**, 1400 (1960).

[55] R. J. Blin-Stoyle and J. LeTourneux, Phys. Rev. **123**, 627 (1961). See, however, A. Altman and W. M. Macdonald (Bull. Am. Phys. Soc., **7**, 17, 1962 and to be published) for a discussion of the magnitude of this effect, assuming the configuration s^4p^{10}.

[56] W. E. Moore, J. N. McGruer, and A. I. Hamburger, Phys. Rev. Letters **1**, 29 (1958); E. Baranger and S. Meshkov, Phys. Rev. Letters **1**, 30 (1958); Errata: Phys. Rev. Letters **1**, 119 (1958); H. A. WeidenMüller (to be published).